

Neural Network Emulator for Atmospheric Chemical ODE

Zhi-Song Liu^{a,b}, Petri Clusius^c, Michael Boy^{b,c}

*^aSchool of Engineering Science, Lappeenranta-Lahti University of Technology
LUT, Lahti, 15110, Finland*

^bAtmospheric Modelling Centre Lahti, Lahti University Campus, Lahti, 15140, Finland

*^cInstitute for Atmospheric and Earth System Research (INAR), The University of
Helsinki, Helsinki, 00014, Finland*

Abstract

Modelling atmospheric chemistry is complex and computationally intense. Given the recent success of Deep neural networks in digital signal processing, we propose a Neural Network Emulator for fast chemical concentration modelling. We consider atmospheric chemistry as a time-dependent Ordinary Differential Equation. To extract the hidden correlations between initial states and future time evolution, we propose ChemNNE, an Attention based Neural Network Emulator (NNE) that can model the atmospheric chemistry as a neural ODE process. To efficiently capture temporal patterns in chemical concentration changes, we implement sinusoidal time embedding to represent periodic tendencies over time. Additionally, we leverage the Fourier neural operator to model the ODE process, enhancing computational efficiency and facilitating the learning of complex dynamical behavior. We introduce three physics-informed loss functions, targeting conservation laws and reaction rate constraints, to guide the training optimization process. To evaluate our model, we introduce a unique, large-scale chemical dataset designed for neural network training and validation, which can serve as a benchmark for future studies. The extensive experiments show that our approach achieves state-of-the-art performance in modelling accuracy and computational speed.

Keywords: atmospheric chemistry, neural network, surrogate, attention, autoencoder

1. Introduction

In the past decades, deep learning has been proven as an efficient data-driven modelling approach that can handle large-scale datasets for complex digital signal processing, like images (Ramesh et al. (2021); Xu et al. (2023)), videos (Sauer et al. (2023)), audio (Radford et al. (2023)), and languages (Sollaiman et al. (2019); OpenAI and et al. (2023); Touvron et al. (2023a,b)). It is intriguing to see if it can benefit chemical modelling problems. There are a number of approaches that use deep neural networks to resolve specific chemical problems, like Su et al. (2024); Goswami et al. (2024). In general, we can take the time evolution of the chemical compound concentration as an Ordinary Differential Equation (ODE), which can be modeled by neural networks. The underlying dynamics of chemical reactions are implicitly captured and optimized through training on data. In this way, we can build neural networks as surrogate models to replace numerical simulations for faster computation. The development of fast neural emulators also helps address the computational bottlenecks in large-scale, high-resolution chemical simulations. Specifically, within global climate models containing millions of grid cells, a fast neural network can accelerate the modeling process at the grid-cell level. This approach significantly reduces computation time by aggregating information from all grid cells to estimate crucial chemical processes relevant to high-resolution climate predictions, enabling near real-time, high-resolution forecasting. While similar research has been conducted in Wu et al. (2023b); Ren et al. (2023), few studies address large-scale atmospheric chemistry modelling or tackle multiple-input-and-multiple-output chemical predictions. Therefore, in this study, we aim at an end-to-end efficient neural network that can model multiple chemical concentrations (49~300 aerosol chemical compounds) over time (one hour). Specifically, given environmental parameters and initial chemical concentrations, the model can predict both the future states of these compounds and the emergence of new compounds from chemical interactions. We evaluate model performance by analyzing temporal concentration changes, using mean squared errors for accuracy and running time for computational efficiency. To interpret the learning ability of attention, we also analyze the key chemical components for their effects and correlations to other compounds. To the best of our knowledge, our proposed ChemNNE is the first neural network-based approach for atmospheric chemical emulation, addressing large-scale multi-compound predictions over time. To summarize, our contributions are:

- We propose the first neural network emulator for atmospheric chemical modelling, designed to predict the future evolution of chemical concentrations based on initial chemical concentrations and environmental parameters.
- To model the inter- and intra-correlations among chemical data, we propose to use time-embedded attention to model the molecule concentration as a learnable time-dependent process.
- We combine the Fourier Neural Operator (FNO) and attention to represent chemical signals in both spatial and frequency domains, facilitating a computationally efficient neural ODE model.
- To better constrain the chemical process, we propose physics-informed losses, including identity loss, derivative loss and mass conservation loss to ensure that the model can predict further future steps without violating the chemistry.
- We conduct extensive experiments on three large-scale tasks, including interperiod, intraperiod and hybridperiod tasks, to show the efficiency of our ChemNNE on various atmospheric chemical problems.

2. Related Work

In atmospheric chemistry, a key focus is studying the oxidation of volatile organic compounds to understand atmospheric transformations. With prior knowledge of the emitted chemical compounds and the main atmospheric reaction paths, researchers analyze atmospheric phenomena from both a micro view, focusing on the concentrations of trace volatile organic compounds (in the ppt or ppb range), and a macro view, examining large-scale effects like cloud formation and air pollution driven by particle formation and growth. Together, these perspectives provide a comprehensive understanding of atmospheric processes. From the mathematical perspective, we study the problem as a time-series problem or partial differential equation (PDE) problem. Given the booming development of deep learning, we will discuss deep learning based chemical modelling in the following sections.

2.1. Deep learning for chemical modelling

The rise of deep learning in the early 2010s has significantly expanded the scope of scientific discovery processes. Advances in GPU technology and innovative algorithms have enabled deep learning and artificial intelligence to integrate scientific knowledge effectively, supporting diverse tasks across multiple domains. AI for chemistry, one of the promising research directions, has recently attracted a lot of researchers for investigation, like weather forecasting, air quality estimation, aerosol chemical interaction, and so on. Graphcast (Lam and et al. (2023)) is one of the promising weather forecasting AI models that uses a graph neural network to predict the global weather with medium-range resolution. Recently, Aurora Bodnar et al. (2024) has revolutionized many facets of climate studies by leveraging vast amounts of data and proposing a foundation model with 1.3B parameters, achieving state-of-the-art performance in weather forecasting. Unlike weather prediction models, atmospheric chemical models examine complex chemical dynamics, capturing interactions and transformations among compounds under physical constraints. It can be very useful for extreme weather study, air pollution prevention and so on. Bassetti et al. Bassetti et al. (2023) propose a conditional emulator via the conditional diffusion model to understand the impact of human actions on the earth system. In parallel, AI’s role in autonomous chemical design and optimization has gained attention. ChemGPT (Boiko et al. (2023)), fine-tuned from large language models like GPT-4 (OpenAI and et al. (2023)), facilitates reaction optimization and experimental automation. Air pollution mitigation, particularly through aerosol chemistry, is another focal area. For example, Hou et al. (2022) employs random forests to analyze PM_{2.5} levels during haze episodes pre- and post-COVID-19 lockdown, while Betancourt et al. (2023) uses graph machine learning to impute missing data in tropospheric ozone measurements, bridging gaps in atmospheric pollutant time series. Additional research has applied machine learning to model other pollutants, such as OH (Zhu et al. (2022)) and NO₂ (Di et al. (2020)). Recently, there has been growing interest in using neural network emulators as fast surrogate models to replace computationally intensive numerical simulations in chemical modelling. Not only can they be built into chemical systems for fast simulation and analysis, but they can also be used in high-resolution global climate modelling. For instance, Bradley et al. (2022) demonstrates the effectiveness of attention models in simulating Atmospheric Chemistry Box Models, achieving speeds over two orders of magnitude faster than traditional solvers. Similarly, Irwin et al. (2022) fine-tunes transformer models

to address cheminformatics tasks. Adie et al. (2024a) utilizes autoencoders and LSTMs for global chemical model simulations, while Liu et al. (2021) introduces a 28-layer residual regression neural network for chemical transport modelling. Despite these advancements, most of these approaches are tailored toward spatiotemporal chemical modelling for short-term weather or air quality analysis. Comprehensive investigations into detailed atmospheric chemical reactions remain relatively unexplored and present a critical area for future research.

2.2. *Neural autoregression and ODE for time series learning*

Given the initial concentrations of chemical compounds and environmental parameters, the overall process of estimating future chemical changes can be framed as either an Ordinary Differential Equation (ODE) approach or as a general time series model, depending on the complexity of temporal dynamics involved. There are two primary approaches for solving time series problems: (1) autoregressive models and (2) ordinary differential equation (ODE)-based processes. Though only a few works are directly related to chemical ODE modelling, summarizing time series works can help establish a foundation for understanding how chemical reactions can be processed and modeled by deep learning.

For autoregression, RNN (Hochreiter and Schmidhuber. (1997)) and attention (Vaswani et al. (2017)) are two major approaches for temporal modelling. RNN-based methods capture sequential temporal variations through recurrent structures, where state transitions are inherently time-dependent. In contrast, attention-based or transformer-based approaches capture global temporal dependencies, identifying specific time steps that are most relevant for accurate future prediction. Specifically, Li et al. (2019); Zhou et al. (2021) propose efficient self-attention models that achieve strong forecasting performance by focusing on scalable attention mechanisms. Wu et al. (2021) introduces Autoformer, which leverages Fast Fourier Transform to compute auto-correlations within time series data, enhancing its ability to capture periodic patterns. FEDformer (Zhou et al. (2022)) further improves forecasting performance by incorporating a mixture-of-experts design, which ensembles specialized knowledge learned from the frequency domain to enhance the model’s ability to capture complex temporal patterns. In cases with partial time series data, TimeNet (Wu et al. (2023a)) proposes the TimesBlock, which projects 1D time series data into a 2D space to capture inter- and intra-time correlations, facilitating more nuanced temporal dependency modelling

for improved forecasting.

Scientific hypotheses in fields like physics or chemistry are often expressed as discrete entities, such as symbolic formulas or chemical compounds. However, these can be represented in a differentiable space, making them suitable for efficient optimization using gradient-based methods. Different from general time series processing, neural ODE/PDE models offer explicit differential systems for optimization. The introduction of neural ODEs (Chen et al. (2018)) has unlocked new avenues for developing novel ODE solvers, with applications spanning physics (Hayat et al. (2020); Portillo et al. (2020)), chemistry (Jiang et al. (2020); Su et al. (2024); Goswami et al. (2024)), and biology (Lu et al. (2021); Pokkunuru et al. (2023)), among other fields. Deep learning-based ODE processes can be broadly categorized into three primary branches: (1) continuous learning (Raissi et al. (2019, 2020); Geneva and Zabarar (2020); Norcliffe et al. (2020)), (2) discrete learning (Zhu et al. (2019); Bhatnagar et al. (2019); Khoo et al. (2020); Bilos̆ et al. (2021); Massaroli et al. (2020); Yildiz et al. (2019)), and (3) neural operators (Li et al. (2020); K. et al. (2024); Li et al. (2023, 2020)). In continuous learning, neural networks are used as domain projectors, mapping data into a continuous latent space to capture global solution patterns. This approach embeds physics-informed loss functions into the training process to ensure that the network’s behavior adheres to the underlying ODE dynamics. Discrete learning, on the other hand, models nonlinear dynamics on mesh grids by utilizing convolutional or graph neural networks.

2.3. Neural operator for spatial and temporal encoding

The recent progress in neural operators for differentiable signal representations (Sitzmann et al. (2020); Saragadam et al. (2022); Lindell et al. (2022)) shows promise for predicting continuous solutions to ODE/PDE systems based on spatiotemporal queries. It is known that using MLP for 1D convolution causes bias in the low frequency domain (Ramasinghe et al. (2024)). Neural operators solve it by providing frequency-aware parameterization, such that high-frequency information will not be suppressed. Siren (Sitzmann et al. (2020)) was one of the first methods to apply sinusoidal functions in neural networks for effective signal reconstruction, creating a foundation for continuous function representation. Fourier Neural Operators (FNO) (Li et al. (2020)) advance this by using the Fast Fourier Transform to map signals in the frequency domain, parameterizing the integral kernel as a straightforward multiplication in Fourier space, significantly reducing

computation. It parameterizes the integral kernel directly in Fourier space as simple multiplication, which is a significant computation reduction. For time series processing, a learnable time encoding system allows for flexible alignment of temporal features, enhancing the model’s adaptability to various time scales and improving temporal resolution. For instance, Spherical Fourier Neural Operator (Bonev et al. (2023)) generalizes the Fourier Transform as a spherical geometry, achieving stable autoregressive on long-term forecasting. Adie et al. (2024b) and Kurth et al. (2023) are the two most recent works that use the Fourier Neural operator for global weather forecasting and chemical modelling. In this work, we aim to explore this technique further, combining it with existing ODE methods to achieve more robust and accurate modelling.

3. Method

3.1. Data preparation

To understand real-world atmospheric chemistry, we need to generate a large-scale dataset for neural network training. Environmental chambers and flow reactors are used to study the complex chemical reactions in the atmosphere under well-controlled conditions. Such experiments have significantly improved our understanding of atmospheric chemical processes and the fate of many volatile organic compounds (VOCs), including anthropogenic pollutants. This has increased the theoretical understanding of atmospheric chemistry, leading to numerical chemical schemes which can describe the time evolution of the atmospheric chemistry. To obtain the dataset, we use the ARCA-box model (Clusius et al. (2022)), a comprehensive toolbox for modelling atmospheric chemistry and aerosol processes. The model can be set up to any kinetic chemistry system, but most often the base chemistry scheme comes from the Master Chemical Mechanism (Jenkin et al. (2015, 1997); Saunders et al. (2003)). We used a subset of the MCM, augmented with the Peroxy Radical Autoxidation Mechanism (Roldin et al. (2019)), which simulates monoterpene autoxidation, crucial in producing low volatility vapors from biogenic volatile organic carbon (BVOC) emissions. The subset was selected so that it contains both biogenically and anthropogenically emitted compounds such as isoprene, monoterpenes, aromatics, alkenes and alkynes, and together with their reaction products contains altogether 3301 compounds and 9530 reactions. The kinetic chemistry system is converted to a system of ODEs using the Kinetic PreProcessor (Sandu et al. (2023)),

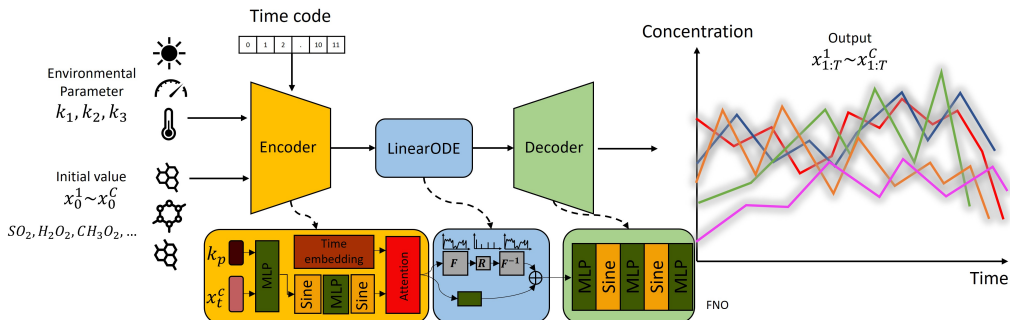


Figure 1: **The proposed ChemNNE for chemical concentration prediction.** It takes the environmental parameters and chemical initial concentration to predict the future chemical reaction process.

and then incorporated in ARCA box and solved numerically to simulate the time series of the reaction products.

To create the dataset, we first selected representative initial concentrations of 49 precursor gas compounds and three environmental conditions: temperature, relative humidity and short-wave radiation, affecting the reaction rates and photochemistry. Chemically related compounds were linked together and varied in tandem, resulting in 15 independently varied groups of initial concentrations. In other words, the variation of initial concentrations of 49 input chemical compounds is determined by 15 independent factors. These factors were selected so that they produced realistic lower and upper bounds of the initial concentrations, and thus obtained 2^{15} combinations of the initial concentrations. Additionally, all simulations were repeated with the environmental variables in the middle values. This produced 3^3 different combinations of physical factors. Hence we obtain total $2^{15} \times 3^3 = 884736$ different chemical reaction samples. For each 1-hour time series, we sample the concentrations every 5 minutes, totalling 12 time steps. During the 1-hour simulation, new chemical compounds are generated, and including the original 49 input chemical compounds, we observe a total of 3301 chemical compounds. For our experiments, we focus on 400 of the most important chemical compounds and ignore others.

3.2. ChemNNE for Atmospheric modelling

To model the atmospheric chemical reaction, we propose the following framework in Figure 1. It consists of three parts: 1) encoder, 2) linearODE,

and 3) decoder. Let us denote the initial chemical concentration as $x_0 \in \mathbb{R}^N$, where N is the number of chemical elements, and the environmental parameters as $k \in \mathbb{R}^O$, where O is the number of environmental factors, e.g., temperature, humidity and radiation. Mathematically, given the time steps $t_i = 0, 1, \dots, T$, the proposed ChemNNE learns a linear ODE function that predicts time-dependent output chemical values $x_t \in \mathbb{R}^N$ as,

$$x_t = \psi \left(\varphi(x_0, k) + \int_{[t_0, t_T]} f(z(t)) dt \right), \text{ where } f(z(t)) = \frac{dz(t)}{dt} \quad (1)$$

In Eq 1, it comprises three components: an encoder φ , the linearODE f , and a decoder ψ . The dynamics of the chemical process are characterized as $z(t)$. Given initial chemical concentration x_0 , we have the latent space initial state $z_0 = \varphi(x_0, k)$, which serves as the initial condition for the ODE. The integral operation is evaluated by the proposed linearODE, which is achieved by the Fourier Neural Operator.

To obtain continuous, differentiable signal representation, we apply sine as a periodic activation function to the chemical input and hidden features, $x_i \rightarrow \phi_i(x_i) = \sin(W_i x_i + b)$, where $W_i \sim \mathcal{U}(-6/\sqrt{N}, 6/\sqrt{N})$, $c \in \mathbb{R}$, as they are continuous changes in the physical world and it is memory efficient to compute the derivatives in the sine space without being constrained by discrete data samples. The initialized weight parameters ensure that the input to each sine activation is normally distributed with a standard deviation of 1. Physically, we can interpret the weights of the sinusoid function as angular frequencies while the biases are phase offsets. Applying the sine function keeps signal amplitude constant while expanding frequency bands for high-frequency modelling. The Encoder is made of sine-based MLP layers and time-dependent attention modules for extracting hidden correlations among different chemical components, and the decoder also uses the sine-based MLP layers for time prediction.

3.2.1. Sinusoid function for time embedding

Observing the chemical reaction simulation, we can see that the chemical compounds usually dynamically change their concentrations over time. This oscillating behavior can resonate with radio frequency modulation, where the true signal can be encoded to the carrier wave by either changing its frequency or amplitude. As pointed out by Sitzmann et al. (2020), using neural networks for continuous and differentiable physical signals is challenging because the neural networks tend to oversmooth the high-frequency details and

do not represent the derivatives of a target signal well. To introduce a differentiable time representation, we propose to use sinusoidal time embedding (Mildenhall et al. (2020)) to the time code, which can be described as follows.

$$\lambda(t) = F_{\Theta} \circ t = (\sin(2\Theta\pi t), \cos(2\Theta\pi t)) \quad (2)$$

Mathematically, given the time steps $t_i = 0, 1, \dots, T$, we project them onto a higher dimensional space \mathbb{R}^{2L} , where $F_{\Theta} \in \mathbb{R}^L$ is the L-length learnable parameters that can define the frequency of the time code. We represent the time as a combination of sine and cosine operators so that the network can learn to adjust the reaction frequency.

3.2.2. Attention for chemical representation

Attention has been widely used in image, video, and language processing. Its success comes from its efficient nonlocal feature representation. For chemical modelling, we also expect an efficient approach that can model the long-term time evolution, so that similar chemical behavior across time or different chemical compounds can be utilized for pattern matching. In order to achieve that, we propose a time-dependent attention module, which can encode and decode the chemical data to the latent space for implicit neural representation. Mathematically, we can define the process as,

$$z_{\lambda}(t) = z_{\lambda}(t) + \text{ffn} \left(z_{\lambda}(t) + \sigma \left(\frac{Q_z K_z^T}{\sqrt{d}} \right) V_z \right) \quad (3)$$

where $z_{\lambda}(t) = \sin[W(z_0) + b] + \lambda(t)$, $Q_z = z_{\lambda}(t)W_Q$, $K_z = z_{\lambda}(t)W_K$, and $V_z = z_{\lambda}(t)W_V$. σ is the softmax function. The W_* is the learnable parameter. z_0 is the output feature of the Sinusoid mapping layer. d is the dimension of the learned feature vector. As depicted in Figure 1, given the latent space chemical features, we apply the Sinusoid mapping first. Then we use the attention module to learn the nonlocal correlations. A feedforward network (ffn) is used to learn the residues for network update. Note that the activation of ffn is also a sine function to preserve the periodic behavior of chemical reactions.

3.2.3. Fourier Neural Operator (FNO)

To explore the derivatives of the chemical reactions, introducing ODE in the neural network can preserve the underlying physical laws. In recent works Chen et al. (2018); Li et al. (2023, 2020), neuralODE, like TorchdiffEq (Chen et al. (2018)), has been used for GPU based ODE approximation.

However, the disadvantage is that it is not numerically stable and rather slow in computation. We propose to further simplify the ODE process as a Neural Fourier Operation. Given the discrete-time representation across multiple chemical components, we use Fourier Transformation to project the signal to the frequency domain and learn the multi-grid nonlinear interactions across temporal and component domains.

$$z_{t+1} = \gamma \left(W z_t + \mathcal{F}^{-1}(R_\phi \cdot (\mathcal{F} z_t)) \right)$$

$$(R_\phi \cdot (\mathcal{F} z_t)) = \sum_{j=1}^{d_v} R_{k,l,j} \mathcal{F} z_{t,k,j}, k = 1, \dots, k_{max}, j = 1, \dots, d_v \quad (4)$$

We lift the signal to the frequency domain, given k frequency modes, we have $\mathcal{F} z_t(k) \in \mathbb{C}^{d_v}$ and $R_\phi(k) \in \mathbb{C}^{d_v \times d_v}$. γ is the nonlinear activation. We define $R_\phi(k)$ as the truncation function that only keeps the maximal number of modes $k_{max} = |k \in \mathbb{Z}_d : |k_j| \leq k_{max,j}, \text{ for } j = 1, \dots, d|$.

The advantages of using FNO for ODE computation are 1) CNN and transformers can only learn on fixed-scale grids and fail to capture the fine scales of multi-scale systems, while FNO is grid-invariant since the operations outside of the Fourier layers act point-wise on the spatial domain, 2) it is faster to use Fourier Transform than convolution, as it is quasilinear, where the full standard integration of n points has complexity $O(n^2)$; 3) the input and outputs of PDEs are discrete functions, so it is efficient to represent them in the Frequency domain for global convolution. In the experiments, we would show the complexity comparisons to demonstrate the efficiency of FNO.

3.2.4. Physics-informed losses.

To train the whole ChemNNE, not only do we utilize the commonly used Mean Squared Errors (MSE) between prediction and ground truth, but we also propose to utilize the first- and second-order derivation, and total mass conservation loss. Mathematically, we can define the overall losses as

$$Loss = \alpha_1 L_{recon} + \alpha_2 L_{d1} + \alpha_3 L_{d2} + \alpha_4 L_{idn} + \alpha_5 L_{mass} \quad (5)$$

In Eq 5, α_1 to α_5 are the weighting parameters that balance all five loss terms. L_{recon} is the reconstruction loss measures the discrepancy between the prediction and ground truth as $L_{recon} = |x(t) - x'(t)|^2$. The first-order gradient loss enforces the predicted trajectories to closely follow the ground

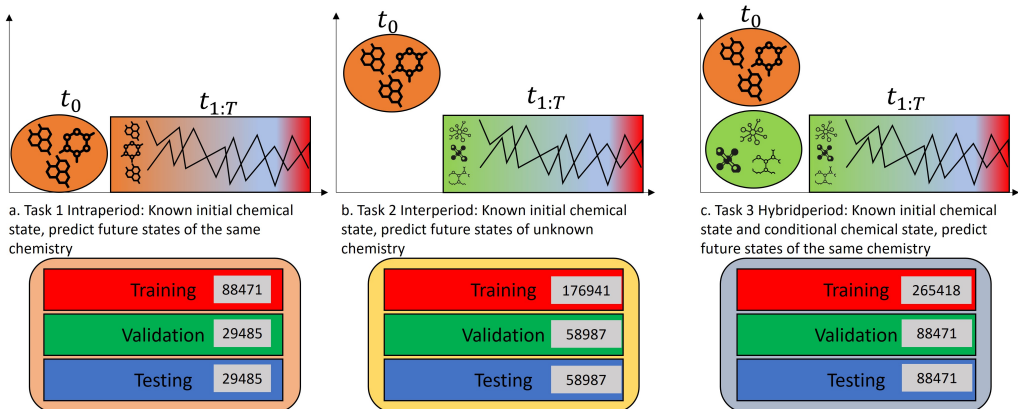


Figure 2: **Three chemical prediction task for model evaluation.**

Tasks	Training	Validation	Testing	Environment input	Chemical input	Chemical output
Task 1	88471	29485	29485	3	48	48
Task 2	176941	58987	58987	3	48	100
Task 3	265418	88471	88471	3	148	300

Table 1: **Data summary of three tasks.**

truth over time as $L_{d1} = |\frac{dx(t)}{dt} - \frac{dx'(t)}{dt}|^2$. Similarly, we can define the second-order gradient loss as $L_{d2} = |\frac{dx^2(t)}{dt^2} - \frac{dx'^2(t)}{dt^2}|^2$. Meanwhile, we can also enforce that the ChemNNE should preserve the initial condition unchanged during the training process. Hence we can define the identity loss as $L_{idn} = |x(t_0) - \psi(\varphi(x(t_0)))|^2$. Finally, we define the total mass conservation loss, ensuring that the mass of the predicted trajectory aligns with the mass of the ground truth at each time step. We have $L_{mass} = |\phi(x(t)) - \phi(x'(t))|^2$, where ϕ is the summation of all chemical components.

3.2.5. Evaluation

To compare the estimations of the proposed ChemNNE against others, we apply the mean absolute errors (MAE) and the root mean squared errors (RMSE) to express the average difference. We also use the mean bias error (MBE) to calculate the estimation bias. The analytic equations for the estimation are:

$$\begin{aligned}
MAE &= \sum_{i=1}^N \frac{|X_i - Y_i|}{N} \\
RMSE &= \sqrt{\sum_{i=1}^N \frac{(X_i - Y_i)^2}{N}} \\
MBE &= \sum_{i=1}^N \frac{X_i - Y_i}{N}
\end{aligned} \tag{6}$$

Furthermore, we also calculate the running time of the proposed model to compare with numerical simulation to see its efficiency, which could indicate how it can be utilized for large-scale modelling.

4. Experiments

4.1. Implementation Details

- **Tasks.** We consider that our proposed ChemNNE can be used as a universal solver that can learn the intra- and inter-correlations among different chemical compounds over time. To test its efficiency, we design three tasks to validate its performance in Figure 2.

- **Task 1: Intraproduct chemical prediction.** Given the same 49 chemical compounds, we take their initial values ($x_0^i, i = 1, 2, \dots, 49$) and environmental parameters k to predict their future states. We use the ARCA box to simulate one-hour changes in chemical concentration and sample the observations every 5 minutes. The objective of the ChemNNE is to predict the results of all 12 time steps, as $x_t^i, i = 1, 2, \dots, 49, t = 1, 2, \dots, 12$.
- **Task 2: Interperiod chemical prediction.** Based on the simulated concentrations of ARCA (concentrations above a defined threshold), we select 100 significant chemical compounds that have high impacts on air quality. We train the proposed model to take the same 49 chemical values ($x_0^i, i = 1, 2, \dots, 49$) and environmental parameters k , and predict the time evolutions of the selected 100 chemical compounds ($y_t^i, i = 1, 2, \dots, 100, t = 1, 2, \dots, 12$).

- **Task 3: Hybridperiod chemical prediction.** Similarly, as Task 2, we further select 300 more new chemical compounds that are generated over time. This is a much more challenging task, and we need additional chemical information to help the model understand the chains of chemical reactions. We design the model to take 49 initial chemical values and 100 new chemical values from Task 2, to output another 300 new chemical compounds at different time steps as $(z_t^i, i = 1, 2, \dots, 300, t = 1, 2, \dots, 12)$.

• **Datasets.** We collected data based on the description in Section 2.1. We ran the simulations on CSC computers¹ for 12 hours. We randomly split the data into non-overlapped training, validation and testing datasets. The data size of all three tasks is summarized in Table 1.

To standardize the data for neural network training, we first take the logarithm of true chemical output to the base 10, then we normalize all data by dividing the maximum value, approximately 31.5. For the environmental parameters, we take the maximum and minimum values to normalize them to $[-1, 1]$. To further increase the data variety, we apply data augmentation to the training set. Specifically, we randomly roll the time evolution of the observation as $\hat{y}_i^t = y_i^{t+\tau}, i = 1, 2, \dots, 100, t = 1, 2, \dots, 12$, where

$$\hat{y}_i^t = \begin{cases} y_i^{t+\tau} & \text{for } \tau < 12 - t \\ y_i^{t+\tau-12} & \text{for } \tau > 12 - t \end{cases} \text{ where } i = 1, 2, \dots, t = 1, 2, \dots, 12 \quad (7)$$

• **Parameter setting.** We train ChemNNE using Adam optimizer with the learning rate of 1×10^{-3} and halved around 20K iterations. The batch size is set to 4096 and ChemNNE is trained for 100k iterations (about 2 hours) on a PC with one NVIDIA V100 GPU using PyTorch deep learning platform. The weighting factors in the total loss are defined empirically as: $\alpha_1 = 1, \alpha_2 = 10, \alpha_3 = 10, \alpha_4 = 1, \alpha_5 = 0.001$.

4.2. Overall comparison with state-of-the-arts

To demonstrate the efficiency of our proposed ChemNNE, we compare it with two state-of-the-art methods: UNet (Williams et al. (2024)), NeuralODE (Chen et al. (2018)), which are widely used in neural ODE/PDE

¹<https://csc.fi/>

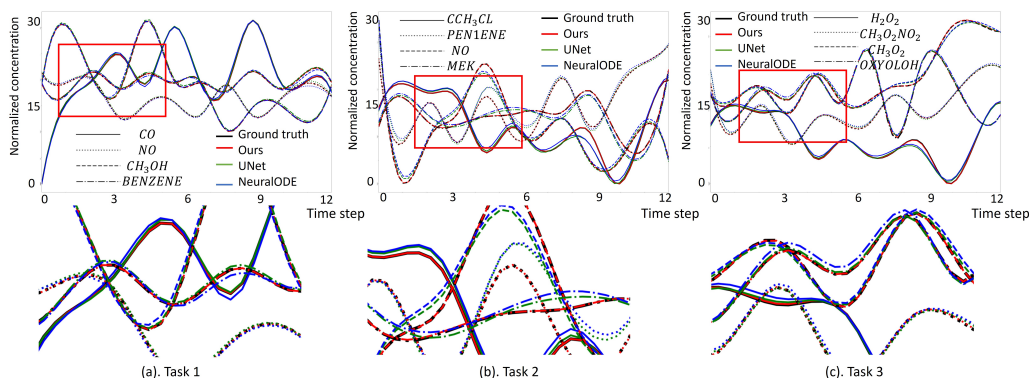


Figure 3: **Visualization of the time evolution of chemistry in Task 1, 2 and 3.** In (a), (b), and (c), we show the ground truth as red lines and the predictions with different colors. We pick four different chemical compounds for comparison, and we also enlarge the region in red boxes to highlight the prediction errors.

processes. The comparison is shown in Table 2. We compare different approaches on both validation and testing datasets in logarithm scales. We also show the model complexity by running time (seconds) and number of Multiply-accumulate operations (MACs). Compared to NeuralODE and UNet, we can observe that using our proposed ChemNNE can achieve the best performance in terms of RMSE, MAE and MBE. For instance, ours can improve the RMSE by about $0.28 \sim 0.41$ in Task 1, $0.1 \sim 0.3$ in Task 2, and $0.14 \sim 0.23$ in Task 3. Comparing different tasks, we can see that the improvements from Task 1 to Task 3 are reduced which also indicates that the modelling

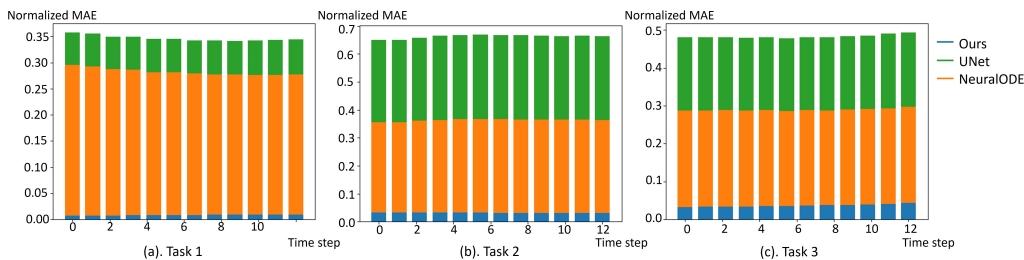


Figure 4: **Visualization of the mean errors of the time evolution in Task 1, 2 and 3.** We average all chemical compounds and show the mean absolute errors between ground truth and other predictions across different time steps.

Task	Model	Validation			Testing			Running time (s)	MACs (M)
		RMSE	MAE	MBE	RMSE	MAE	MBE		
Task 1	UNet	0.4210	0.3292	0.2232	0.4267	0.3316	0.2152	5.15e-5	10.45
	NeuralODE	0.3959	0.2741	0.0003	0.3958	0.2738	0.0002	1.06e-4	10.95
	Ours	0.0194	0.0086	-1.9e-5	0.0652	0.0441	-0.0028	5.12e-5	13.77
Task 2	UNet	0.4283	0.2984	0.0163	0.4291	0.2988	0.0166	5.06e-5	14.11
	NeuralODE	0.2136	0.1244	0.0094	0.2144	0.1247	0.0074	1.26e-4	12.13
	Ours	0.1156	0.0312	-0.0037	0.1174	0.0316	-0.0037	5.55e-5	13.94
Task 3	UNet	0.3096	0.1933	-0.0009	0.3090	0.1932	-0.0009	9.74e-5	45.03
	NeuralODE	0.2102	0.1079	-0.0015	0.2086	0.1078	-0.0016	2.18e-4	42.03
	Ours	0.0748	0.0357	0.0003	0.0749	0.0359	0.0003	1.07e-4	44.34

Table 2: **Compare state-of-the-art methods on three tasks for chemical concentration prediction.** We test different methods on both validation and testing sets. For all metrics, the lower the values, the better prediction is achieved.

difficulty is increased when more unknown chemical components are estimated. From the computation complexity, ours has a comparable number of operations as the other two and achieves a similar running speed. As the baseline, the numerical chemical model takes 0.05 seconds to run one simulation. It indicates that ours can be used as a fast emulator to accelerate the chemical modelling process. In practical applications, neural surrogate models can detect and respond to subtle climate changes far more quickly than traditional numerical models. This rapid detection has the potential to significantly reduce human and economic costs associated with catastrophic climate events. For visualization, we take different results on Tasks 1, 2, and 3 and visualize them in Figure 3. In tasks 1, 2, and 3, there are over 100 different chemical compounds, which makes it difficult to visualize them all in one figure. We randomly pick 4 individual chemical compounds and draw them in different line styles (solid, dotted, dashed, dash-dot). For each compound, we show the predictions of UNet, NeuralODE and ours in green, blue and red color. The ground truth value is shown in black color. We enlarge the red-box regions to demonstrate better the differences between ground truth and predictions. We can see that using ours can accurately align with the ground truth, while UNet and NeuralODE still produce distinct gaps between the ground truth. For a complete chemical compound comparison, you can find the figures in the supplementary material.

Meanwhile, we calculate the mean absolute prediction errors across dif-

Components					Task 1			Task 2			Task 3		
AE	Attn	Time emb	Sinusoid	FNO	RMSE	MAE	MBE	RMSE	MAE	MBE	RMSE	MAE	MBE
✓					0.3776	0.1876	0.0155	0.3976	0.2995	0.0368	0.5113	0.4010	0.0301
✓	✓				0.1252	0.0662	0.0044	0.2615	0.1589	0.0152	0.2455	0.1675	0.0089
✓		✓			0.3240	0.1665	0.0147	0.3589	0.2745	0.0235	0.5012	0.3370	0.0125
✓			✓		0.2256	0.1825	0.0035	0.1956	0.0899	0.0168	0.4888	0.3412	0.0115
✓				✓	0.0707	0.0486	0.0033	0.1389	0.0785	-0.0082	0.0789	0.0386	-0.0023
✓	✓	✓			0.0649	0.0441	-0.0029	0.1373	0.0675	0.0068	0.0768	0.0375	-0.0010
✓	✓	✓	✓		0.0201	0.0109	0.0041	0.1182	0.0324	0.0031	0.1201	0.0328	0.0032
✓	✓	✓	✓	✓	0.0194	0.0086	-1.9e-5	0.1156	0.0312	-0.0037	0.0748	0.0357	0.0003

Table 3: **Comparison on different key components of our proposed ChemNNE** . We report the results on validation datasets and for all metrics, lower values mean better performance.

ferent chemical compounds and summarize errors by time steps. In Figure 4, we compare different approaches to three different tasks. We can see that ours achieves the lowest errors across different time steps in all tasks. We can also observe that the further time steps, the higher the errors we get, which fits our assumption that long-term chemical prediction produces higher uncertainty. Depending on the difficulty of different tasks, we can also see that task 2 has the overall highest errors, and task 1 has the lowest errors. It is interesting to note that Task 3 uses 100 chemical compounds actively involved in the chemical reactions as additional input. This allows the model to better understand the correlations between the initial chemical values and the 300 new chemical compounds. For instance, knowing the concentration of *OH* (one of the 100 significant chemical compounds for air quality) can help predict the concentration changes of *C7300H* and *OXYLOOH* (two of the 300 predicted chemical compounds). As a result, the model for Task 3 performs slightly better than that for Task 2.

4.3. Ablation studies

We conduct several ablations to test the key components of the proposed ChemNNE and report the results in Table 3.

We use the validation dataset of all three Tasks to demonstrate the effects of different key components, including AE (AutoEncoder), attention (attn), time embedding (Time emb), Sinusoid, FNO, and their combinations. Using AE is our baseline. We can see that the last row is our final model, which shows the best performances in all metrics. Individually, we can see that using attention and FNO can achieve the most improvements by approximately

Task		MSE (baseline)	MSE+Derivs	MSE+Derivs+Idn	MSE+Derivs+Mass	MSE+Derivs+Idn+Mass
Task 1	RMSE	0.0315	0.0268	0.0225	0.0210	0.0194
	MAE	0.0126	0.0102	0.0094	0.0089	0.0086
	MBE	0.0008	2.9e-5	3.4e-5	2.8e-5	-1.9e-5
Task 2	RMSE	0.1876	0.1820	0.1502	0.1501	0.1156
	MAE	0.0589	0.0566	0.0408	0.0386	0.0312
	MBE	0.0089	0.0091	-0.0076	0.0064	-0.0037
Task 3	RMSE	0.0896	0.0895	0.0820	0.0766	0.0748
	MAE	0.0523	0.0510	0.0461	0.0447	0.0357
	MBE	0.0015	0.0015	0.0008	0.0010	0.0003

Table 4: **Comparison on different loss terms of our proposed ChemNNE** . We report the results on the validation dataset and we can see that the combination of all losses achieves the best performance.

0.1 \sim 0.4 in terms of RMSE. Using time embedding and Sinusoid can also improve the RMSE by about 0.01 \sim 0.2.

To further demonstrate the effect of the key components of attention and FNO, we visualize the training loss convergences in Figure 5. We enlarge the region within the red box and highlight it at the upper center to illustrate the loss differences. Compared to Unet and NeuralODE, we can see that ours with attention and/or FNO achieves the fastest convergence speed and lowest training loss.

Finally, we train our proposed ChemNNE with different loss combinations, so that we can validate the effects of using physics-informed losses for model optimization. As the baseline, we train the model with MSE loss (L_{recon}), and then we individually add other losses to retrain the model, including first- and second-order derivative losses (Derivs), identity loss (IDN), and mass conservation loss (Mass). In Table 4, we show the RMSE, MAE, and MBE results on three tasks. Our observations are: 1) from columns 2 and 3, we can see that using identity and mass conservation losses have a more significant loss drop, about 0.03 \sim 0.1 in RMSE, 2) using derivative loss has more visible effects on Task 1 than Task 2 and 3 because Task 1 is intraperiod chemical prediction, that is, the derivative can better constrain the chemical reaction process for accurate estimation.

4.4. Statistical analysis

To study in depth the proposed ChemNNE on the ability of chemical modelling, we study the error distributions among different chemical com-

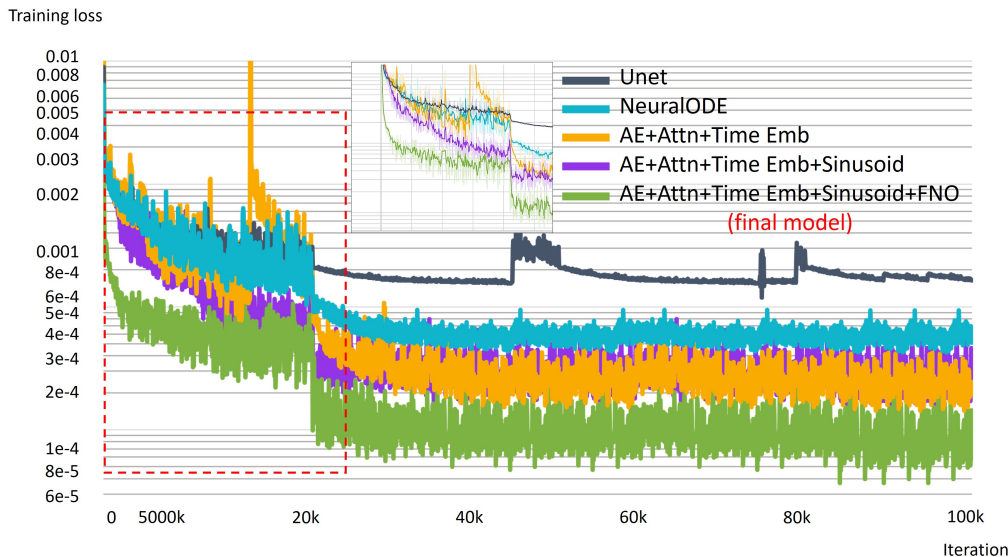


Figure 5: **Training loss comparison among ours and others.** We show different approaches in different colors. We enlarge the red-boxed region and display it at the upper center. We can see the improvements of using our proposed ChemNNE in both convergence speed and final loss.

ponents and time steps, so that we can see whether the model can estimate the patterns for each individual component, as well as long-term regression. In Figure 6, we show the error distribution in Task 1. We can see that 1) the model performs unevenly on different chemical components in terms of means and variances, and 2) the errors increase when predicting further steps in the future.

For Tasks 2 and 3, we have a much larger number of chemical components, 100 to 300 chemical components, for computation. To efficiently demonstrate the model performance, we show the 2D heatmap of mean and variance distributions on the validation datasets. Figure 7 and Figure 8 show the mean and variance of error distributions in all three tasks. The brighter the color, the higher the errors the model produces. From Figure 7, we can observe that the average performance differences depend on the specific chemical components. From Figure 8, we can see that the error variances vary because of the time steps. The farther the future step to predict, the higher the variances the model gets. The patterns also match our observations in Figure 6.

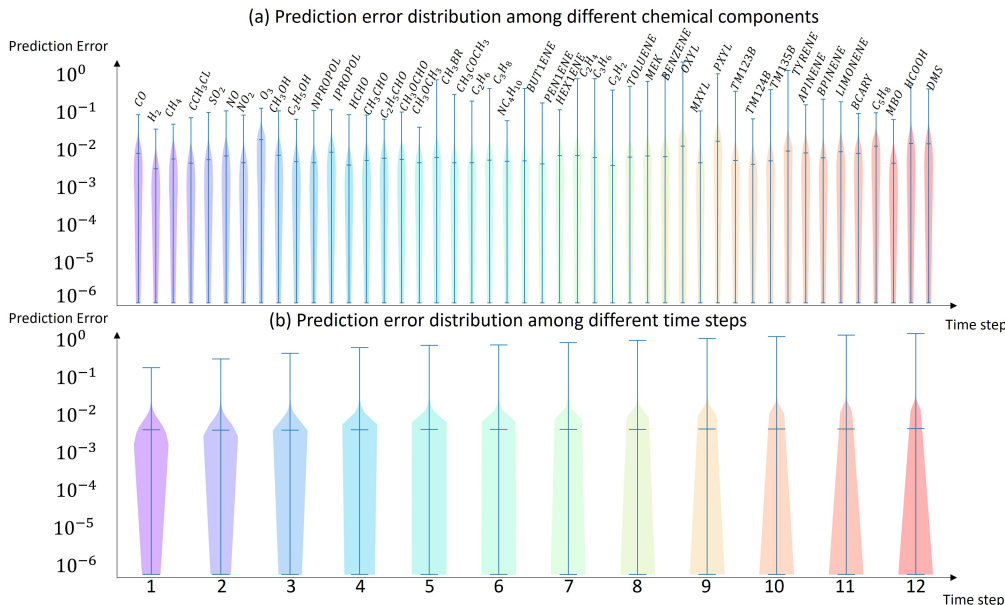


Figure 6: **Validation error distribution visualization via violin plots.** We show the error distributions (using the logarithm scale for better visualization) of different chemical components (a), and different time steps (b). The narrower the color shades, the smaller the error distributions.

Specifically, we are interested in the chemistry that the model fails to predict well. In Task 1, the top five highest errors come from O_3 , $OXYL$, $PXYL$, $HCOOH$, DMS . Ozone (O_3) is one of the main oxidants in the atmosphere and reacts with many compounds. Therefore its predictions are related to the concentrations of many other compounds. 1,2-dimethylbenzene ($OXYL$) and 1,4-dimethylbenzene ($PXYL$) are aromatics which react mainly with the hydroxyl radical (OH). OH is formed inside the model and is the most important oxidant of the atmosphere during daytime and reactive towards nearly all compounds. The uncertainty for $OXYL$ and $PXYL$ is mainly related to the performance of OH and the same is the reason for dimethylsulphide (DMS) and formic acid ($HCOOH$). For Task 2, the top four highest errors come from $HOC_2H_4CO_2H$, $PXYLCO_2H$, $KLIMONIC$, $C_{88}CO_2H$. For Task 3, the top two highest errors come from $OXYQOOH$, $LMLKBCO$. All these compounds are higher-order reaction products of our initial compounds and are formed after several reactions with ozone, the nitrate and the hydroxyl

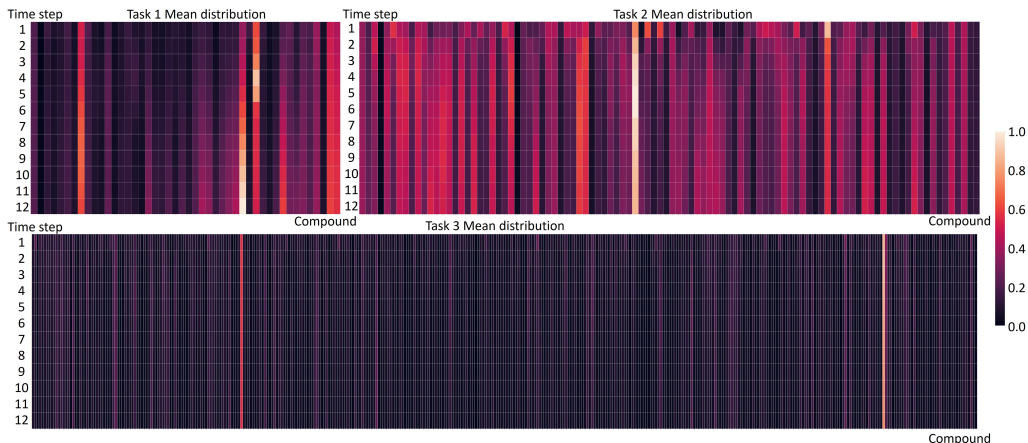


Figure 7: **Mean distribution of validation errors of three tasks.** We show the mean values of error distributions on three tasks, where the horizontal axis represents different chemical components and the vertical axis represents different time steps.

radical. The most promising way to decrease the uncertainties of these compounds is to increase our training data set in the future.

5. Conclusion

In this paper, we propose the first work on a neural network emulator for fast chemical modelling, dubbed ChemNNE . We utilize the numerical simulation to generate a large-scale chemical dataset which is used to train the proposed ChemNNE , so that it can learn the hidden inter- and intra-correlations among chemical molecules. We propose to combine attention and neural ODE operations to model the time-dependent chemical reactions. Meanwhile, we lift the neural ODE as a Fourier domain convolution such that we can efficiently model the global continuous ODE. The time embedding and Sinusoid operators also help model the oscillation patterns to mimic the concentration changes of chemistry. To demonstrate the efficiency and effectiveness of the proposed model, we test it on three tasks, including intraperiod, interperiod and hybridperiod chemical predictions. Extensive experiments show that ours achieves the best performance in both accuracy and running speed. This work paves a new direction in AI for atmospheric chemistry, and we will continue to explore graph neural networks, equivalent

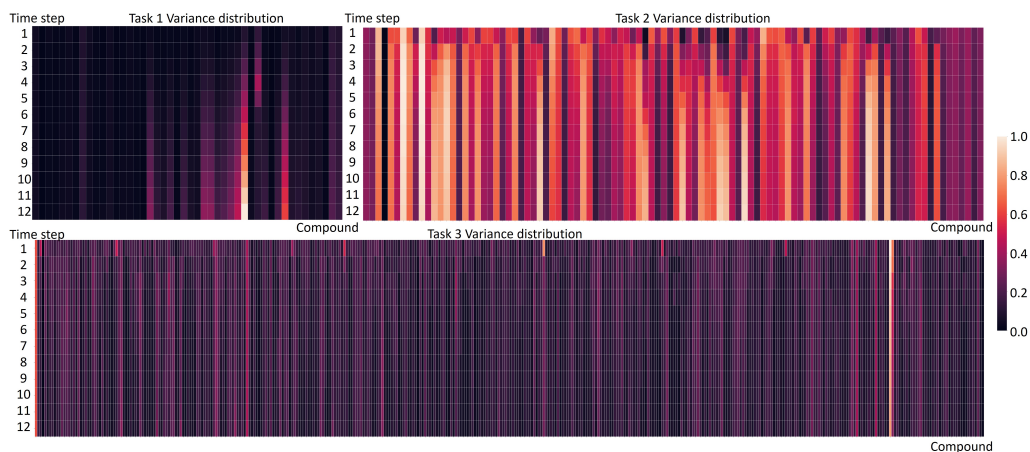


Figure 8: **Variance distribution of validation errors of three tasks.** We show the variance values of error distributions on three tasks, where the horizontal axis represents different chemical components and the vertical axis represents different time steps.

neural networks, and other advanced models to integrate chemical knowledge for physics-informed processing.

References

- Adie, J., Chin, C.S., Li, J., See, S., 2024a. Gaia-chem: A framework for global ai-accelerated atmospheric chemistry modelling, in: Proceedings of the Platform for Advanced Scientific Computing Conference, Association for Computing Machinery, New York, NY, USA. URL: <https://doi.org/10.1145/3659914.3659927>, doi:10.1145/3659914.3659927.
- Adie, J., Chin, C.S., Li, J., See, S., 2024b. Gaia-chem: A framework for global ai-accelerated atmospheric chemistry modelling, in: Proceedings of the Platform for Advanced Scientific Computing Conference. doi:10.1145/3659914.3659927.
- Bassetti, S., Hutchinson, B., Tebaldi, C., Kravitz, B., 2023. Diffesm: Conditional emulation of earth system models with diffusion models. International Conference on Learning Representation .
- Betancourt, C., Li, C.W.Y., Kleinert, F., Schultz, M.G., 2023. Graph machine learning for improved imputation of missing tropospheric ozone data.

- Environmental Science & Technology 57, 18246–18258. doi:10.1021/acs.est.3c05104. PMID: 37661931.
- Bhatnagar, S., Afshar, Y., Pan, S., Duraisamy, K., Kaushik, S., 2019. Prediction of aerodynamic flow fields using convolutional neural networks 64, 525–545.
- Biloš, M., Sommer, J., Rangapuram, S.S., Januschowski, T., Günnemann, S., 2021. Neural flows: Efficient alternative to neural odes. Advances in neural information processing systems 34, 21325–21337.
- Bodnar, C., Bruinsma, W.P., et al., 2024. Aurora: A foundation model of the atmosphere. arXiv 2405.13063.
- Boiko, D., MacKnight, R., Kline, B., et al., 2023. Autonomous chemical research with large language models. Nature 624, 570–578.
- Bonev, B., Kurth, T., Hundt, C., et al., 2023. Spherical fourier neural operators: learning stable dynamics on the sphere, in: Proceedings of the 40th International Conference on Machine Learning.
- Bradley, H., Abraham, N.L., Nowack, P., McNeall, D., 2022. Transformers for fast emulation of atmospheric chemistry box models, in: NeurIPS 2022 Workshop on Tackling Climate Change with Machine Learning. URL: <https://www.climatechange.ai/papers/neurips2022/74>.
- Chen, R.T.Q., Rubanova, Y., Bettencourt, J., Duvenaud, D., 2018. Neural ordinary differential equations , 6572—6583.
- Clusius, P., Xavier, C., Pichelstorfer, L., Zhou, P., Olenius, T., Roldin, P., Boy, M., 2022. Atmospherically relevant chemistry and aerosol box model – arca box (version 1.2). Geoscientific Model Development 15, 7257–7286.
- Di, Q., Amini, H., Shi, L., Kloog, I., Silvern, R., Kelly, J., Sabath, M.B., Choirat, C., Koutrakis, P., Lyapustin, A., Wang, Y., Mickley, L.J., Schwartz, J., 2020. Assessing no2 concentration and model uncertainty with high spatiotemporal resolution across the contiguous united states using ensemble model averaging. Environmental Science & Technology 54, 1372–1384. doi:10.1021/acs.est.9b03358. PMID: 31851499.

- Geneva, N., Zabaras, N., 2020. Modeling the dynamics of pde systems with physics-constrained deep auto-regressive networks 403.
- Goswami, S., Jagtap, A.D., Babae, H., Susi, B.T., Karniadakis, G.E., 2024. Learning stiff chemical kinetics using extended deep neural operators, in: CHAME.
- Hayat, M.A., Stein, G., Harrington, P., Lukic, Z., Mustafa, M., 2020. self supervised representation learning for astronomical images. *The Astrophysical Journal Letters* .
- Hochreiter, S., Schmidhuber, J., 1997. Long short-term memory. *Neural Comput.* .
- Hou, L., Dai, Q., Song, C., Liu, B., Guo, F., Dai, T., Li, L., Liu, B., Bi, X., Zhang, Y., Feng, Y., 2022. Revealing drivers of haze pollution by explainable machine learning. *Environmental Science & Technology Letters* 9, 112–119. doi:10.1021/acs.estlett.1c00865.
- Irwin, R., Dimitriadis, S., He, J., Bjerrum, E.J., 2022. Chemformer: a pre-trained transformer for computational chemistry. *Machine Learning: Science and Technology* 3, 015022. URL: <https://dx.doi.org/10.1088/2632-2153/ac3ffb>, doi:10.1088/2632-2153/ac3ffb.
- Jenkin, M., Young, J., Rickard, A., 2015. The mcm v3.3.1 degradation scheme for isoprene. *Atmospheric Chemistry and Physics* 15.
- Jenkin, M.E., Saunders, S.M., Pilling, M.J., 1997. The tropospheric degradation of volatile organic compounds: a protocol for mechanism development. *Atmospheric Environment* 31, 81–104.
- Jiang, C., Esmailzadeh, S., Azizzadenesheli, K., et al., 2020. Mesh-freeflownet: a physics-constrained deep continuous space-time super-resolution framework, in: *Proceedings of the International Conference for High Performance Computing, Networking, Storage and Analysis*.
- K., N., Li, Z., Liu, B., et al., 2024. Neural operator: learning maps between function spaces with applications to pdes. *J. Mach. Learn. Res.* 24.
- Khoo, Y., Lu, J., Ying, L., 2020. Solving parametric pde problems with artificial neural networks 32, 421–435.

- Kurth, T., Subramanian, S., Harrington, P., Pathak, J., Mardani, M., Hall, D., Miele, A., Kashinath, K., Anandkumar, A., 2023. Fourcastnet: Accelerating global high-resolution weather forecasting using adaptive fourier neural operators, in: Proceedings of the Platform for Advanced Scientific Computing Conference. doi:10.1145/3592979.3593412.
- Lam, R., et al., 2023. Learning skillful medium-range global weather forecasting. *Science* 382, 1416–1421.
- Li, S., Jin, X., Xuan, Y., Zhou, X., Chen, W., Wang, Y.X., Yan, X., 2019. Enhancing the locality and breaking the memory bottleneck of transformer on time series forecasting. *Advances in neural information processing systems* 32.
- Li, Z., Kovachki, N., Azizzadenesheli, K., Liu, B., Bhattacharya, K., Stuart, A., Anandkumar, A., 2020. Fourier neural operator for parametric partial differential equations.
- Li, Z., Kovachki, N.B., Choy, C., Li, B., Kossaifi, J., Otta, S.P., Nabian, M.A., Stadler, M., Hundt, C., Azizzadenesheli, K., Anandkumar, A., 2023. Geometry-informed neural operator for large-scale 3d PDEs, in: Thirty-seventh Conference on Neural Information Processing Systems.
- Lindell, D.B., Van V., D., Park, J.J., Wetzstein, G., 2022. Bacon: Band-limited coordinate networks for multiscale scene representation, in: IEEE/CVF Conference on Computer Vision and Pattern Recognition (CVPR), pp. 16231–16241.
- Liu, C., Zhang, H., Cheng, Z., Shen, J., Zhao, J., Wang, Y., Wang, S., Cheng, Y., 2021. Emulation of an atmospheric gas-phase chemistry solver through deep learning: Case study of chinese mainland. *Atmospheric Pollution Research* 12, 101079. URL: <https://www.sciencedirect.com/science/article/pii/S1309104221001458>, doi:<https://doi.org/10.1016/j.apr.2021.101079>.
- Lu, L., Jin, P., Pang, G., et al., 2021. Learning nonlinear operators via deepnet based on the universal approximation theorem of operators, in: *Nat Mach Intell*, pp. 218–229.

- Massaroli, S., Poli, M., Park, J., Yamashita, A., Asama, H., 2020. Dissecting neural odes. *Advances in Neural Information Processing Systems* 33, 3952–3963.
- Mildenhall, B., Srinivasan, P.P., Tancik, M., Barron, J.T., Ramamoorthi, R., Ng, R., 2020. Nerf: Representing scenes as neural radiance fields for view synthesis, in: *ECCV*.
- Norcliffe, A., Bodnar, C., Day, B., Simidjievski, N., Liò, P., 2020. On second order behaviour in augmented neural odes. *Advances in neural information processing systems* 33, 5911–5921.
- OpenAI, et al., 2023. Gpt-4 technical report. *International Conference on Learning Representation* .
- Pokkunar, A., Rooshenas, P., Strauss, T., Abhishek, A., Khan, T., 2023. Improved training of physics-informed neural networks using energy-based priors: A study on electrical impedance tomography, in: *International Conference on Learning Representation*.
- Portillo, S.K., Parejko, J.K., Vergara, J.R., Connolly, A.J., 2020. Dimensionality reduction of sdss spectra with variational autoencoders. *The Astrophysical Journal* 45.
- Radford, A., Kim, J., Xu, T., et al., 2023. Robust speech recognition via large-scale weak supervision, in: *Proceedings of the 40th International Conference on Machine Learning*.
- Raissi, M., Perdikaris, P., Karniadakis, G.E., 2019. Physics-informed neural networks: A deep learning framework for solving forward and inverse problems involving nonlinear partial differential equations 378, 686—707.
- Raissi, M., Yazdani, A., Karniadakis, G.E., 2020. Hidden fluid mechanics: Learning velocity and pressure fields from flow visualizations 367, 1026—1030.
- Ramasinghe, S., Macdonald, L., Lucey, S., 2024. On the frequency-bias of coordinate-mlps, in: *Proceedings of the 36th International Conference on Neural Information Processing Systems*.

- Ramesh, A., Pavlov, M., Goh, G., Gray, S., Voss, C., Radford, A., Chen, M., Sutskever, I., 2021. Zero-shot text-to-image generation, in: Meila, M., Zhang, T. (Eds.), Proceedings of the 38th International Conference on Machine Learning, pp. 8821–8831.
- Ren, P., Rao, C., Liu, Y., Ma, Z., Wang, Q., Wang, J.X., Sun, H., 2023. Physr: Physics-informed deep super-resolution for spatiotemporal data. *Journal of Computational Physics* , 112438.
- Roldin, P., Ehn, M., Kurtén, T., et al., 2019. The role of highly oxygenated organic molecules in the boreal aerosol-cloud-climate system. *Nat Commun* 4370.
- Sandu, A., Sander, R., et al., 2023. An adaptive auto-reduction solver for speeding up integration of chemical kinetics in atmospheric chemistry models: implementation and evaluation within the kinetic pre-processor (kpp) version 3.0.0. *JAMES* 15.
- Saragadam, V., LeJeune, D., Tan, J., Balakrishnan, G., Veeraraghavan, A., Baraniuk, R.G., 2022. Wire: Wavelet implicit neural representations, in: arXiv preprint arXiv:2301.05187.
- Sauer, A., Lorenz, D., Blattmann, A., Rombach, R., 2023. Adversarial diffusion distillation. arXiv:2311.17042.
- Saunders, S.M., Jenkin, M.E., Derwent, R.G., Pilling, M.J., 2003. Protocol for the development of the master chemical mechanism, mcm v3 (part a): tropospheric degradation of non-aromatic volatile organic compounds. *Atmospheric Chemistry and Physics* 3, 161–180.
- Sitzmann, V., Martel, J.N., Bergman, A.W., Lindell, D.B., Wetzstein, G., 2020. Implicit neural representations with periodic activation functions, in: Proc. NeurIPS.
- Solaiman, I., Brundage, M., Clark, J., Askill, A., Herbert-Voss, A., Wu, J., Radford, A., Wang, J., 2019. Release strategies and the social impacts of language models. arXiv preprint arXiv:1908.09203 .
- Su, J., Ma, J., Tong, S., Xu, E., Chen, M., 2024. Multiscale attention wavelet neural operator for capturing steep trajectories in biochemical systems, in: AAAI Conference on Artificial Intelligence, pp. 15100–15107.

- Touvron, H., Lavril, T., Izacard, G., Martinet, X., Lachaux, M.A., Lacroix, T., Rozière, B., Goyal, N., Hambro, E., Azhar, F., Rodriguez, A., Joulin, A., Grave, E., Lample, G., 2023a. Llama: Open and efficient foundation language models. arXiv preprint arXiv:2302.13971 .
- Touvron, H., Martin, L., Stone, K., Albert, P., et al, 2023b. Llama 2: Open foundation and fine-tuned chat models. arXiv preprint arXiv:2307.09288 .
- Vaswani, A., Shazeer, N., Parmar, N., Uszkoreit, J., Jones, L., Gomez, A., Polosukhin, I., 2017. Attention is all you need. Advances in neural information processing systems , 5998–6008.
- Williams, C., Falck, F., Deligiannidis, G., Holmes, C., Doucet, A., Syed, S., 2024. A unified framework for u-net design and analysis, in: Proceedings of the 37th International Conference on Neural Information Processing Systems.
- Wu, H., Hu, T., Liu, Y., Zhou, H., Wang, J., Long, M., 2023a. Timesnet: Temporal 2d-variation modeling for general time series analysis .
- Wu, H., Xu, J., Wang, J., Long, M., 2021. Autoformer: Decomposition transformers with auto-correlation for long-term series forecasting. Advances in neural information processing systems .
- Wu, Z., Wang, J., Du, H., et al., 2023b. Chemistry-intuitive explanation of graph neural networks for molecular property prediction with substructure masking. Nat Commun 14.
- Xu, Z., Sangineto, E., Sebe, N., 2023. Stylerdalle: Language-guided style transfer using a vector-quantized tokenizer of a large-scale generative model, in: Proceedings of the IEEE/CVF International Conference on Computer Vision (ICCV), pp. 7601–7611.
- Yildiz, C., Heinonen, M., Lahdesmaki, H., 2019. Ode2vae: Deep generative second order odes with bayesian neural networks. Advances in Neural Information Processing Systems 32.
- Zhou, H., Zhang, S., Peng, J., Zhang, S., Li, J., Xiong, H., Zhang, W., 2021. Informer: Beyond efficient transformer for long sequence time-series forecasting. AAAI Conference on Artificial Intelligence .

- Zhou, T., Ma, Z., Wen, Q., Wang, X., Sun, L., Jin, R., 2022. Fedformer: Frequency enhanced decomposed transformer for long-term series forecasting .
- Zhu, Q., Laughner, J.L., Cohen, R.C., 2022. Combining machine learning and satellite observations to predict spatial and temporal variation of near surface oh in north american cities. *Environmental Science & Technology* 56, 7362–7371. doi:10.1021/acs.est.1c05636. pMID: 35302754.
- Zhu, Y., Zabaras, N., Koutsourelakis, P.S., Perdikaris, P., 2019. Physics-constrained deep learning for high-dimensional surrogate modeling and uncertainty quantification without labeled data 394, 56–81.

Supplementary material: Neural Network Emulator for Atmospheric Chemical ODE

Zhi-Song Liu^{a,b}, Petri Clusius^c, Michael Boy^{b,c}

^a*School of Engineering Science, Lappeenranta-Lahti University of Technology
LUT, Lahti, 15110, Finland*

^b*Atmospheric Modelling Centre Lahti, Lahti University Campus, Lahti, 15140, Finland*

^c*Institute for Atmospheric and Earth System Research (INAR), The University of
Helsinki, Helsinki, 00014, Finland*

1. Network architecture

The network detail is shown in Figure 5. We show the dimension of feature maps to indicate the computation process. N is the number of chemical compounds. B is the batch size. For different tasks, we have different N . As introduced in Section 3.2, the encoder consists of several MLP layers followed by Sine activation functions. It takes as input the initial chemical concentration value and the environmental factors to learn a joint hidden feature vector $B \times 256$. Then we expand and repeat it to $B \times 256 \times 12$, where 12 is the total time steps it learns to predict. A self-attention module learns to extract non-local features for better feature representation. The sinusoid mapping projects the time code to the dimension of $B \times 256 \times 12$, then we multiply it with the feature vector and pass it to the LinearODE module. The linearODE module is made of several FNO blocks, which process the input feature by global convolution. Finally, the decoder also contains a set of MLP layers with sine activation functions to produce final time prediction.

2. Visualization of chemical prediction

In Section 4.2 of the main manuscript, we show the prediction comparisons of four individual chemical compounds. In Section 4.3, we also show statistical comparisons among different methods. However, it would be interesting to show an overall comparison of all chemical compounds. Please note that we have three different tasks, and each task processes different numbers

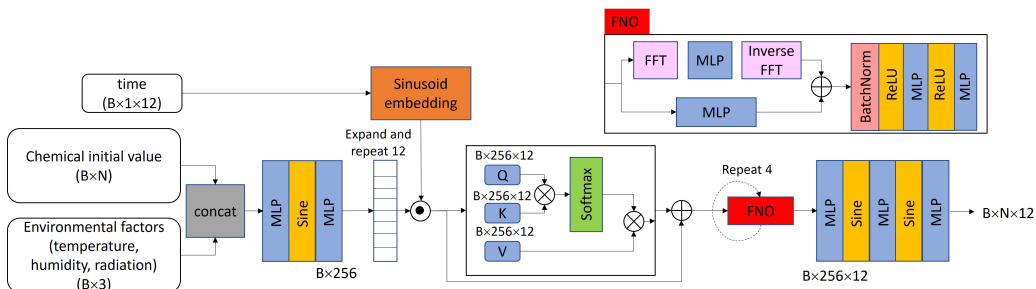


Figure 1: **The detail of the proposed ChemNNE for chemical concentration prediction.** We show the dimension of feature maps to indicate the computation process. The encoder contains a set of MLP layers with sine activation functions. The output hidden feature is further processed by the self attention module. The decoder also consists of several MLP layers with sine activations. In the middle, we use 4 FNO blocks to learn the inter- and intra-correlations among different chemical reactions and time evolutions.

of chemical compounds. For task 1, the proposed ChemNNE predicts 49 different chemical elements. For tasks 2 and 3, it needs to predict 100 and 300 chemical compounds. In the following figures, we use dashed black lines to represent the ground truth data, and solid color lines to represent our predictions. We can see that using ours can accurately align with the ground truth. For Task 2 and 3, we show the results in Figure 4. We can see that the color lines are overlapped with the dashed black lines, which indicates that our predictions align well with the ground truth values.

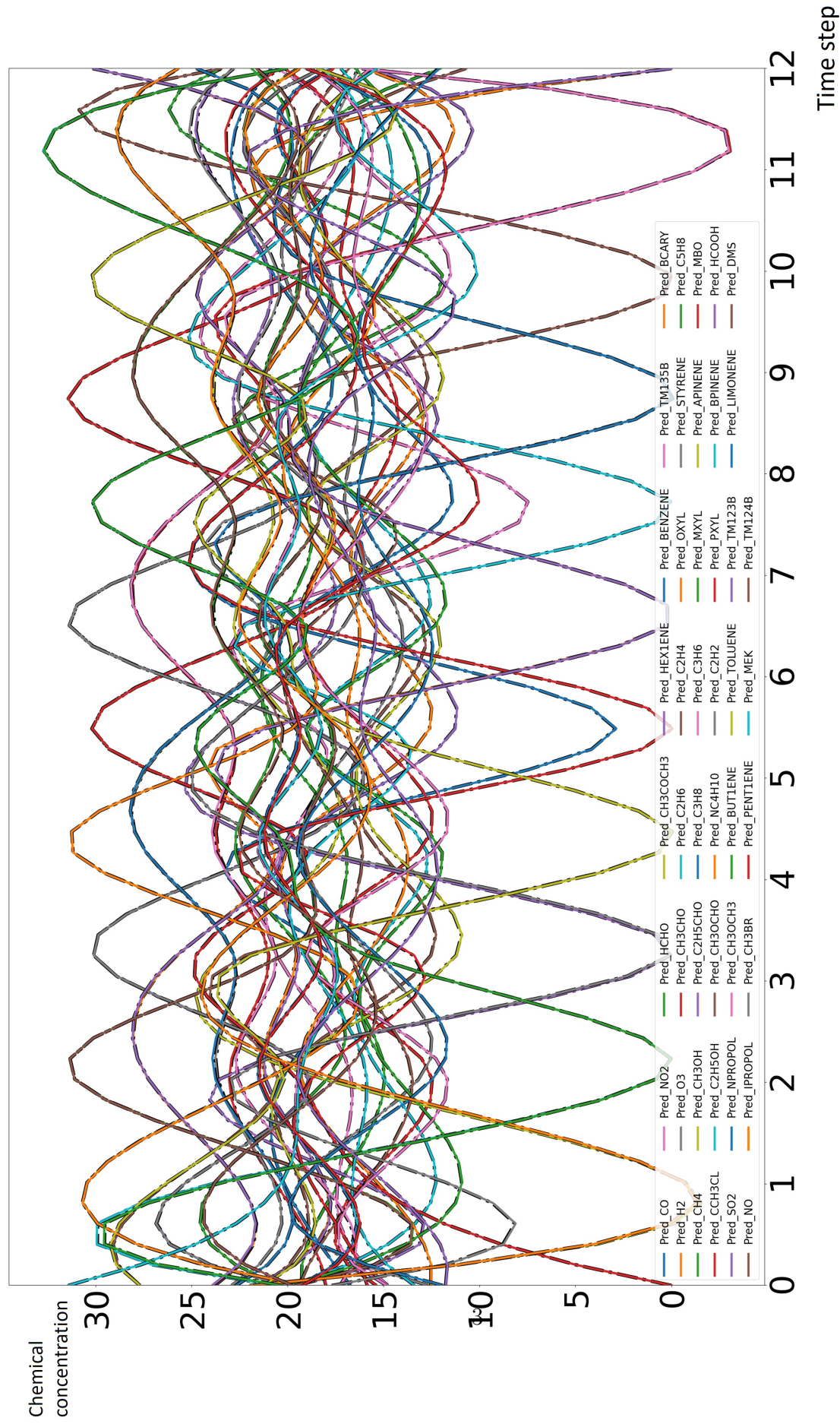


Figure 2: **The overall chemical concentration prediction on Task 1.** We show the ground truth as dashed black lines and the predictions as solid lines with different colors.

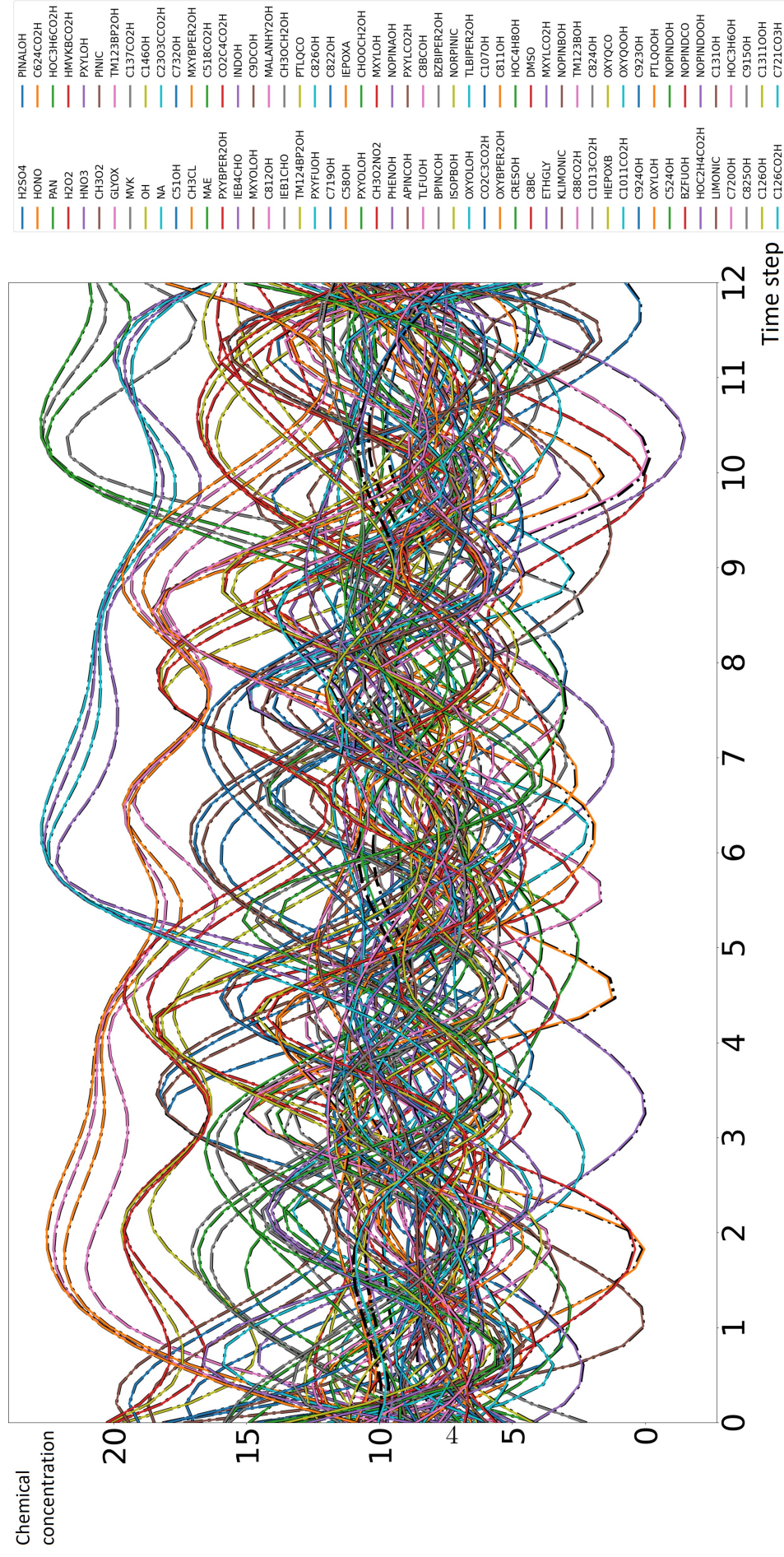


Figure 3: The overall chemical concentration prediction on Task 2. We show the ground truth as dashed black lines and the predictions as solid lines with different colors.

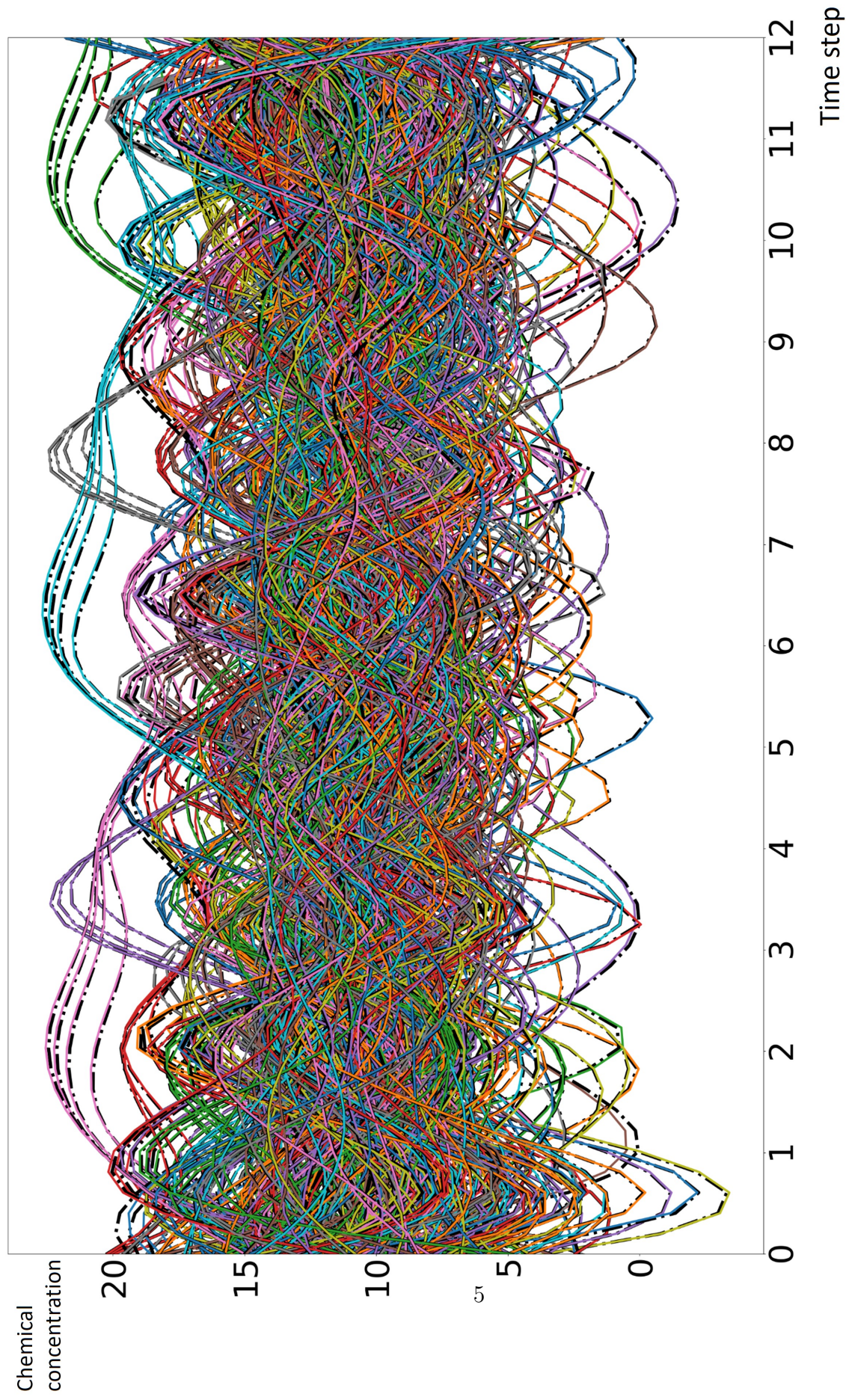


Figure 4: **The overall chemical concentration prediction on Task 3 [Data].** We show the ground truth as dashed black lines and the predictions as solid lines with different colors.

H2SO4	PINALOH	C137CO3H	C6220OH	BZEMUCCO3H	C817CO3H	BCALCOH	MEKANO3
HONO	C624CO2H	C825CO	C141CO3H	OXYLOOH	LIMAOH	INB1HPCHO	MMALANHY
PAN	HOC3H6CO2H	TM123BP0OH	C1410OH	HMVKA0OH	MCATEC10OH	DMK2OH	LIMCNO3
H2O2	HMVKB02H	TM124OLOOH	IEACO3H	BCALO0H	C89CO2H	C514CO23OH	SC4H90OH
HN03	PXYLOH	MXYQ0OH	C9200OH	MXYMUCCO3H	HMACO2H	C1011CO	C148CO
CH3O2	PINIC	ISOP340OH	C7190OH	BPINAOH	BZBIPEROOH	NBUTOL	LIMBNO3
GLYOX	TM123BP2OH	MALDALCO3H	LMKAN03	OXYMUCCO3H	C8160OH	C5DIALOH	BCALNO3
MVK	C137CO2H	C8220OH	MXCTEC10OH	C890OH	C719NO3	C926OH	CH3OCH2NO3
OH	C146OH	C923CO3H	C624CO3H	TLBIPEROOH	C450OH	LIMALBOH	C6250OH
NA	C2303CCO2H	C235C6CO3H	H3C25CCO3H	TM135BP0OH	C816CO3H	C818CO	OXYQONE
C51OH	C732OH	MMALNHYOOH	C1390OH	C10120OH	OXYBPEROOH	BCBCO	LMLKBO
CH3CL	MXYBPER2OH	PXYOLOOH	OXYOLOOH	C6240OH	PXYMUCCO3H	BCALBOH	SC4H9NO3
MAE	C518CO2H	PXYLCO3H	C970OH	C622CO3H	C1160OH	C2H50OH	C1480OH
PXYBPER2OH	CO2C4CO2H	T124CT10OH	EPXMDLCO3H	HCOCH2CO3H	TM124B0OH	C824CO	C6270OH
IEB4CHO	INDOH	C1370OH	C126CO3H	C822CO3H	C7310OH	C1510OH	BC5O20OH
MXYOLOH	C9DCOH	TLEMUCOOH	PERPROACID	C920CO3H	LIMCOOH	C8200OH	C131NO3
CH12OH	MALANHY2OH	C1070OH	C1360OH	MBOAOH	NOPINCOOH	EPXM2DCO2H	C1460OH
IEB1CHO	CH3OCH2OH	C517CO3H	CH3OCH20OH	EPXDLCO2H	MXYOLOH	C51NO3	NC3H7NO3
TM124BP2OH	PTLQCO	C8260OH	C8240OH	C7320OH	TM124BPOOH	C6280OH	NBUTOLBOOH
PXYFUOH	C826OH	TM124MU0OH	C131CO3H	C6H5CH20OH	C9150OH	C52OH10OH	IPROPOL2H
C719OH	C822OH	BZEMUCOOH	C13130OH	OXYMUCCO2H	C732CO3H	C6H50OH	MC6CO2OH
C58OH	IEPOXA	MXYFU0OH	BPINAOH	CH3500OH	PERBUACID	HO3C4NO3	CHOOCH20OH
PXYOLOH	CHOOCH2OH	PHENO0H	C9180OH	C727CO3H	C1450OH	LMLKBOOH	LMLKNO3
CH3O2NO2	MXYOLOH	C7170OH	CO23C4CO3H	C9260OH	EPXDLCO3H	C4CHOB0OH	CH2BROOH
PHENO0H	NOPINAOH	HOPINONIC	C9210OH	C1080OH	C1060OH	HYETHO2H	C7210OH
APINCOH	PXYLCO2H	TM135MU0OH	BZEMUCCO2H	MXYMUCCO2H	C1310OH	NAPINBOOH	C7160OH
TLFUOH	C8BCOH	C1420OH	PXYMUCCO0H	C6140OH	C5140OH	C6OH5NO3	PTLQONE
BPINCOH	BZBIPER2OH	CO3C4CO2H	C980OH	T123CT10OH	PXYBPEROOH	BCLKCO	C5DICAROOH
ISOPBOH	NORPINIC	BZFUCO	TM135OLOOH	C8120OH	C731CO3H	BCALBCO	CH30OH
OXYOLOH	TLBIPER2OH	C7300OH	C9230OH	NBPINBOOH	H3C2C4CO3H	LIMALNO3	APINBOOH
CO2C3CO2H	C107OH	C729CO3H	C8230OH	C147CO	TM123B0OH	C7340OH	HPC52CO3H
OXYBPER2OH	C811OH	OXYMUCCO0H	C1260OH	C1470OH	C5160OH	C726CO50OH	C66NO35OH
CRE5OH	HOC4H8OH	MALNHYOHCO	BCCOOH	C9190OH	C88CO3H	NC4H9NO3	CH3NO3
C8BC	DMSO	C7200OH	C7290OH	ALLYLOH	HVMK	NAPINAOOH	PE1ENEBNO3
ETHGLY	MXYLCO2H	C7200OH	HC4CCO2H	LIMALOOH	INAHPCHO	CH35CHO	C717NO3
KLIMONIC	NOPINBOH	C5C0DBC03H	OCATEC10OH	STYRENOOH	APINBCO	C6125CO	C5110OH
C88CO2H	TM123BOH	CH3CO3H	C1270OH	MXY10OH	C4COMOH3OH	LIMALBCO	ACO2H
C1013CO2H	C824OH	PERPENACID	C823CO3H	C6230OH	LIMBCO	MCOCOMOOH	LIMBOOH
HIEPOXB	OXYQCO	EPXMDLCO2H	C10130OH	LMKAOH	LIMLACO	LIMALBO	C146CO
C1011CO2H	OXYQOOH	C729CO2H	C9170OH	TMB0OH	LIMALAOH	BCLKBOOH	C923NO3
C924OH	C923OH	C10110OH	NORLIMOOH	C656OH	LMLKAOH	EPXM2DCO3H	C8190OH
OXYLOH	PTLQOOH	C6H5CO3H	C734CO	C626CO2H	INDHPCHO	HYPROP02H	CHOMOHCO3H
C524OH	NOPINDOH	APINCOOH	C8170OH	PXYFU0OH	C126CO	C10100OH	C823NO3
BZFUOH	NOPINDCO	APINBOH	C8130OH	C626CO3H	C615CO2OH	C1520OH	NLIMOOH
HOC2H4CO2H	NOPINDOOH	CO3C4CO3H	C510OH	HOC3H6CO3H	C726CO3OH	C7220OH	MXYQONE
LIMONIC	C131OH	PERPINONIC	MXYBPEROOH	PXYMUCCO2H	C7236CO	H3C25C6OH	C9240OH
C720OH	HOC3H6OH	BCAOH	C811CO3H	C136CO3H	C4M2AL2OH	NBUTOLAOOH	C622NO3
C825OH	C915OH	C5C0140OH	C9160OH	MXYMUCOOH	C9DC	C413COOOH	IPRHOCO2H
C126OH	C13110OH	CATEC10OH	ISOPDOH	PCATEC10OH	LMLKBOH	HO5C60OH	C817NO3
C126CO2H	C721CO3H	TM123MU0OH	M3BU3ECO3H	C1430OH	BCALAOH	MBOANO3	C8180OH

Figure 5: The overall chemical concentration prediction on Task 3 [Label].
The label information for Task 3.